INORGANIC CHEMISTRY FRONTIERS

RESEARCH ARTICLE

View Article Online
View Journal | View Issue

Check for updates

Cite this: *Inorg. Chem. Front.*, 2023, **10**, 3058

Exploring the origin of the high electro-catalytic activity for nitrate-to-ammonia conversion on electrodeposited Ni/Ru hydroxide hybrids†

Fengling Zhou *[a] and Chenghua Sun *[b]

Received 28th March 2023,
Accepted 15th April 2023

DOI: 10.1039/d3qi00568b

rsc.li/frontiers-inorganic

Nitrate electro-reduction reaction (NITRR) offers a promising alternative approach for ammonia synthesis under mild conditions. Our previous studies have shown that electrodeposited Ni/Ru hydroxide hybrid exhibits highly catalytic NITRR activity. Therefore, this study focuses on investigating the origin of the high activity on Ni/Ru hydroxide hybrid by comparing it with drop-cast Ru nanoparticles on nickel foam, which show much lower activity for NITRR. This was attributed to the interaction between Ru and the nickel substrate formed during electrodeposition. To host electrodeposited Ni/Ru hydroxide hybrid nanoparticles, we used a series of nickel foams with varying amounts of surface-oxidized nickel layers prepared by heat treatments. The introduction of moderate oxidized nickel layers in Ni/Ru hydroxide hybrid electrodes increased the interactions between Ru and the Ni species, and the synergistic effect further promotes nitrate-to-ammonia conversion. However, excessive increases in oxidized nickel layers lead to a deterioration in catalytic performance.

Published on 19 april 2023. Downloaded on 10/11/2024 21:07:09.

Introduction

Ammonia has significant importance beyond being a fertilizer for agriculture and a raw material for the chemical industry. Its advantages in transport have made it a promising energy fuel. However, the current Haber–Bosch production process for ammonia, which is one of the most important chemical reactions in the world, consumes a significant amount of energy and contributes to approximately 1.5% of CO_2 emissions annually, causing global environmental problems. Therefore, alternative routes for ammonia synthesis under mild conditions have been sought for decades.[1] While electrochemical synthesis of ammonia is promising due to ambient reaction conditions;[2] the ultra-strong N≡N covalent bond makes it extremely challenging to convert N_2 to NH_3 with sufficient activity and efficiency.[3] Various catalysts have been developed for direct nitrogen-to-ammonia synthesis,[4] but the faradaic efficiency and yield rates are still far below the expectations for industrial applications.

Another strategy for ammonia synthesis is to electro-catalytic oxidation of N_2 to NO_3^-, followed by further electro-reduction of NO_3^- to NH_3 ($NO_3^- + 8e^- + 6H_2O \rightarrow NH_3 + 9OH^-$).[5] Unlike N_2, nitrate contains single nitrogen and N≡N breakage is not required prior to ammonia formation. More importantly, nitrate, as a worldwide industrial waste, has been identified as a major pollutant responsible for gas emissions, acid rain or photochemical smog,[6] causing various health-threatening consequences.[7] Against this background, effective electro-reduction of NO_3^- to ammonia not only provides an alternative route for NH_3 production, but also converts nitrate waste into valuable chemicals.[8] So far, traditional catalysts based on Ti,[9] Cu[8b,10] or Co,[11] have been developed for NO_3 electro-reduction, and the energy efficiency for ammonia synthesis is often as high as 90% at low current densities,[10a,12] while the challenge is the decrease in reaction selectivity when targeting high production yield at high current.[13] To address this issue, Ru with oxygen-doped nanoclusters has been demonstrated to have excellent activity for electrochemical nitrate reduction reactions,[14] especially when tensile strains associated with oxygen doping have been introduced, offering ammonia-production rates of 3.25×10^{-7} mol s^{-1} cm^{-2} at −0.8 V *vs.* RHE.[14a] Such success highlights the outstanding activity of Ru nanoparticles, but such catalysts suffer from the efficiency drop at high potentials (*e.g.* down to 55.8% at −0.8 V (ref. 14*a*)). Recently, we have demonstrated a facile and low-cost electrodeposition process for the synthesis of highly active bimetallic Ru–Ni catalysts for nitrate-to-ammonia conversion,

[a]*Guangdong Provincial Key Laboratory of Distributed Energy Systems, Dongguan University of Technology, Dongguan, 523808, China. E-mail: zhoufl@dgut.edu.cn*
[b]*Department of Chemistry and Biotechnology and Centre for Translational Atomaterials, Swinburne University of Technology, Hawthorn, VIC 3122, Australia. E-mail: chenghuasun@swin.edu.au*

† Electronic supplementary information (ESI) available. See DOI: https://doi.org/10.1039/d3qi00568b

This journal is © the Partner Organisations 2023

Published on 19 april 2023. Downloaded on 10/11/2024 21:07:09.

exhibiting high nitrate-to-ammonia conversion rate ($1.4 \pm 0.1 \times 10^{-6}$ mol s^{-1} cm^{-2} at −0.6 V *vs.* RHE) with almost 100% ammonia selectivity.[15] In this study, we conducted further investigations on the catalyst structure to better understand the high efficiency of nitrate-to-ammonia conversion. We compared electrodes prepared by drop-cast Ru nanoparticles onto pristine nickel foam with electrodeposited Ni/Ru hydroxide hybrid. Our results show that the drop-cast electrode exhibited significantly lower nitrate-to-ammonia conversion efficiency than the electrodeposited electrodes. In addition, a series of nickel foams with varying degree of surface oxidation, achieved through heat treatments at room temperature to 500 °C in H_2 or Ar gas, serve as 3D substrates to host electrodeposited Ni/Ru hydroxide hybrid nanoparticles. We observed that the Ni/Ru hydroxide hybrid on deeper oxidized nickel layers exhibited improved NITRR performance compared to those with less oxidized layers. However, further increase in the degree of oxidized nickel layers led to a deterioration of the catalytic performance. Comparison of these results revealed that moderate oxidized nickel substrates played a key role in the observed catalytic activity, leading to formation of Ru–O–Ni matrix, which enhanced the NITRR activity with respect to pristine or reduced nickel surface.[16]

Results and discussion

Firstly, a partially oxidized Ru nanoparticle was drop-cast on a pristine nickel foam (pNF) and labelled as Ru-LPD/pNF (as detailed in ESI†). Additionally, the Ru–Ni bimetallic hybrid electrodes were also prepared by a cycle voltammetry (CV) electrodeposition method on pNF by 25 CVs, denoted as Ru-25CV/pNF (as detailed in ESI†).

The NITRR activity of the catalysts was evaluated by the cyclic voltammograms (CV) and the liner scan voltammetry (LSV) measured in 1.0 M KOH with and without $NaNO_3$. All the voltages reported in this work were converted by referencing to the reverse hydrogen electrode (RHE) and can calculated by E (V) = E° + 0.059 × pH + 0.2415 with pH = 14. Fig. 1a and b presents the electrochemical performance of the Ru-25CV/pNF and Ru-LPD/pNF. Upon the addition of NO_3^-, the onset potentials shift from −0.05 V to 0.15 V, indicating a good response to the nitrate reduction reaction. The current density of the Ru–Ni hybrids increases significantly at potentials below 0.2 V (Fig. 1a, red solid line) and exhibits a much higher cathodic current than that of the Ru-LPD/pNF. Since the performance is related to the active surface area and Ru loading amount in the electrodes, the electrochemical active surface area (ECSA) and the Ru loadings were measured to normalize the current as shown in Fig. 1b. Notably, the normalized currents of the Ru-25CV/pNF by the Ru loading (Fig. 1c) or the ECSA (Fig. 1d) are much higher than that of the Ru-LPD/pNF, further confirming the high NITRR activity of the electrodeposited Ru–Ni hybrids.

Furthermore, the nitrate-to-ammonia conversion efficiency was significantly improved in the Ni–Ru hybrids, as shown in

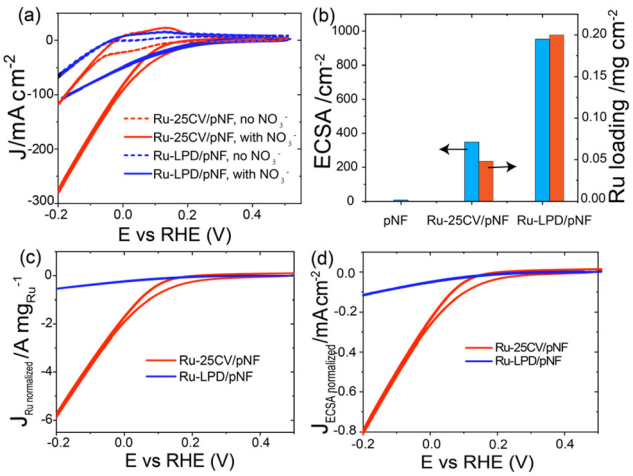

Fig. 1 (a) The cyclic voltammetry (CV) of Ru-LPD/pNF and Ru-25CV/pNF measured in Ar saturated-1.0 M KOH with and without 1.0 M $NaNO_3$ at the scan rate of 10 mV s^{-1}. (b) The ECSA calculated from the capacitance data in detailed in ESI and Fig. S1,† and Ru loading amount of Ru-LPD/pNF and Ru-25CV/pNF analysed by ICP-OES. (c) The Ru loading amount normalized and (d) the ECSA normalized CV of Ru-LPD/pNF and Ru-25CV/pNF from a based on the ECSA and Ru loading in b.

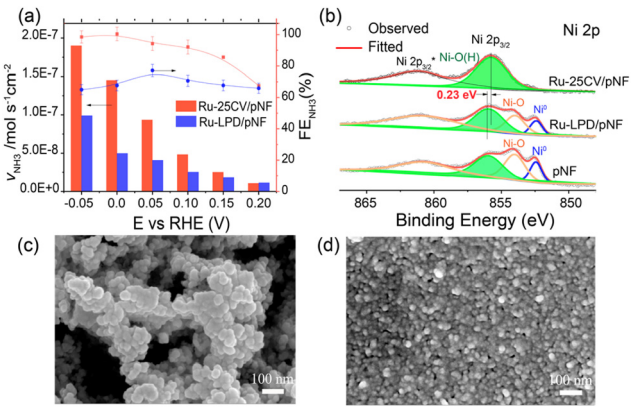

Fig. 2 (a) The ammonia yield rate (V_{NH_3}) and ammonia current faradaic efficiency (FE_{NH_3}) of Ru-LPD/pNF and Ru-25CV/pNF, measured in 1.0 M KOH with 1.0 M $NaNO_3$. (b) The XPS Ni 2s spectra of the Ru-LPD/pNF and Ru-25CV/pNF. The SEM images of (c) Ru-LPD/pNF and (d) Ru-25CV/pNF.

Fig. 2a. For instance, by keeping the FE_{NH_3} at almost 100%, the Ru-25CV/pNF (Fig. 2a, red column) produced ammonia at a rate of 1.5×10^{-7} mol s^{-1} cm^{-2} at 0 V, which is three times higher than that of the Ru-LPD/pNF (0.5×10^{-7} mol s^{-1} cm^{-2} with FE = 68%). In order to investigate the origin of the high catalytic activity of the electrodeposited Ru–Ni hybrid for NITRR, the Ru-25CV/pNF sample was characterized by transmission electron microscopy (TEM), scanning electron microscopy (SEM) and X-ray photoelectron spectroscopy (XPS) as detailed in Fig. 2b–d and Fig. S2–6.† The Ru-25CV/pNF sample exhibits a layer of nanoclusters with the nanoparticle size at 5–10 nm (Fig. 2d and Fig. S2, 3†), which is smaller than

Published on 19 april 2023. Downloaded on 10/11/2024 21:07:09.

the particle size of the Ru-LPD (~30 nm, Fig. 2c and Fig. S4†). The XPS results of the Ru 3d and O 1s (Fig. S5 and 6†) indicate the presence of both Ru^0 and Ru–O bonds in the Ru-25CV/pNF and the Ru-LPD, which are considered crucial for efficient nitrate-to-ammonia conversion.[15]

Regarding the Ni states, the XPS spectra of Ni 2p for the Ru-LPD/pNF are similar to those of the pristine NF (Fig. 2b), showing characteristic peaks of Ni^0, NiO and Ni-OH. This suggests that the drop casting of Ru-LPD onto pNF does not significantly affect or alter the surface states of the initial nickel foam. However, in the case of electrodeposition, only the Ni-OH peak can be observed, which can be assigned to NiOOH,[17] implying that NiO on the pristine NF surface has been converted to NiOOH ($Ni^{2+} \rightarrow Ni^{3+}$), probably due to the Ni/Ru interfacial bonding between Ru and Ni species formed during electrodeposition. This is supported by the shift of the Ni-OH peak to lower energy by 0.23 eV on the electrodeposited Ru-25CV/pNF with respect to the initial nickel foam substrate and the Ru-LPD/pNF.[15] The interfacial bonding between Ni and Ru is likely to contribute to the improved NITRR performance for the Ru–Ni hybrids, as evidenced by their higher nitrate reduction current (Fig. 1a and c, d). Whereas, the Ru-LPD/pNF exhibits a lower FE_{NH_3} and ammonia yield rate (Fig. 2a).

The Ni/Ru interfacial bond is likely formed due to the presence of nickel oxide species, which are typically present on the surface of the pristine nickel foam as indicated in Fig. 2b and in the literature.[18] As shown in the synthesis section, the oxidized layer can be reduced by heat treatment in H_2 flow (Fig. S7†) and labelled as rNF. The amount of electrodeposited Ru on rNF (0.055 mg cm^{-2}) is slightly more than that on pNF (0.048 mg cm^{-2}), and the former has a higher ECSA (Fig. 3a and b). It is important to investigate whether HER side reaction has been effectively suppressed to achieve high energy efficiency, as a high current response in a reaction does not necessarily lead to a high ammonia production rate. Using the reduced sample for demonstration (Ru-25CV/rNF Fig. 3c, blue line), its HER activity is much higher than that of Ru-25CV/pNF, indicating a good suppression of HER in the Ru-25CV/pNF. Both Ru-25CV/rNF and Ru-25CV/pNF demonstrate excellent response to NO_3^- addition, but the reaction current of Ru-25CV/rNF is much lower than that of Ru-25CV/pNF as indicated in Fig. 3d. This suggests that nickel oxide, rather than metallic nickel, is favourable for NITRR.

Furthermore, to gain a better understanding of the correlation between the NITRR activity and the nickel oxide interlayer, Ru supported on nickel foam with deeper oxidized surfaces (oxidized nickel foam, oNF) was investigated. The oNFs show nanoparticles merging on the surface, while the rNF and pNF surfaces are smoother (Fig. S8†). As identified by Ni 2p XPS spectra (Fig. S7†), NiO and nickel hydroxide (Ni-OH) species appear on the nickel foam surfaces,[19] which can be manipulated by controlled oxidation, as previously reported.[10a] The Ru film deposited on the oNF, has a much thinner Ru layer than the rNF and pNF supported Ru film (Fig. S9†), which is in consistent with the much lower Ru loading on the oNFs (0.005 mg cm^{-2} for oNF500 and 0.013 mg cm^{-2} for oNF300, respectively) as indicated by the ICP-OES results (Fig. 3b).

In terms of the electrochemical performance, both the Ru-25CV/oNF300 and Ru-25CV/oNF500 show lower current density than the Ru-25CV/pNF in KOH (Fig. 4a), indicating better suppressed HER in the deeper oxidized NF supported Ru. In the electrolyte with NO_3^-, the Ru-25CV/oNF300 has a similar current to the Ru-25CV/pNF, while the Ru-25CV/oNF500 shows a slight decrease in the current density (Fig. 4b). This is probably due to significant decreases of the ECSA and the Ru loading amount on the oNF supports (Fig. 3a

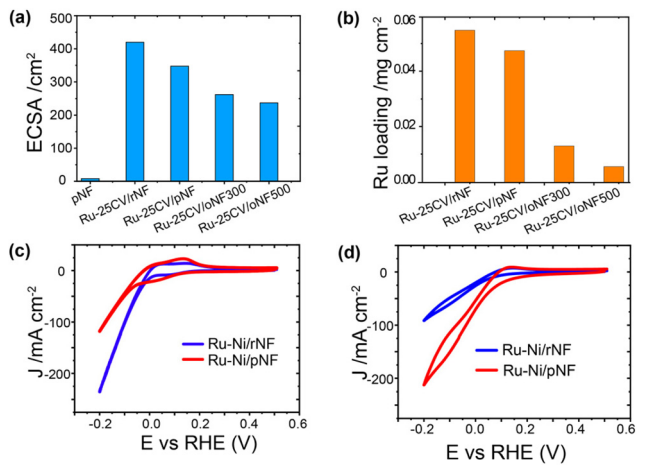

Fig. 3 (a) The measured ECSA and (b) electrodeposited Ru loading amount on different substrates for 25 CVs deposition. The LSV of Ru-25CV/pNF and Ru-25CV/rNF in Ar saturated (c) 1.0 M KOH and (d) 1.0 M KOH with 0.1 M $NaNO_3$ at the scan rate of 10 mV s^{-1}.

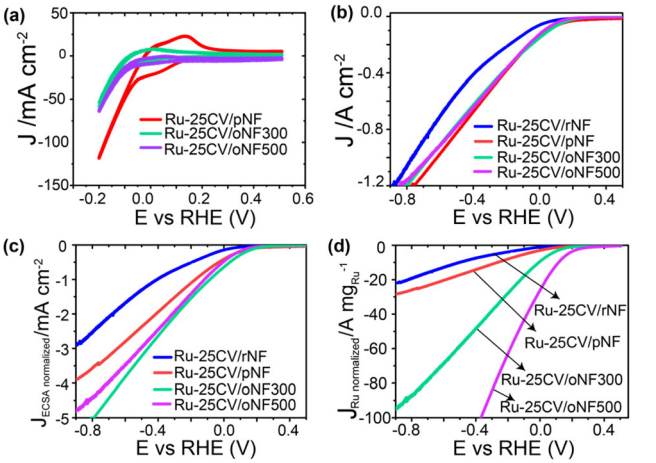

Fig. 4 (a) The LSV of electrodes in Ar saturated 1.0 M KOH. The (b) original, (c) the ECSA normalized and (d) the Ru amount normalized LSV of Ru-25CV supported on different NF, and (d) the ammonia yield rate (V_{NH_3}) and ammonia current faradaic efficiency (FE_{NH_3}) for Ru-25CV on different NF, measured in Ar saturated-1.0 M KOH with 1.0 M $NaNO_3$ at the scan rate of 10 mV s^{-1}.

This journal is © the Partner Organisations 2023

Published on 19 april 2023. Downloaded on 10/11/2024 21:07:09.

and b). To further explore the intrinsic catalytic activity, the electrochemical performances were normalized by the ECSA or the Ru loading mass. It is interesting to note that the normalized LSVs by either the ECSA (Fig. 4c) or the Ru loading mass (Fig. 4d) show significantly enhanced normalized current densities in Ru-25CV/oNF300 and Ru-25CV/oNF500, compared to those with less nickel oxide layers (Ru-25CV/pNF and Ru-25CV/rNF).

A high current response in a reaction does not necessarily lead to a high ammonia production rate as electrons can be consumed by HER side reaction. The ammonia production performances were examined in Ar saturated-1.0 M KOH with 1.0 M $NaNO_3$ at varied potentials (Fig. 5a). At high cathodic potentials (up to −0.9 V), the FE_{NH_3} and V_{NH_3} follow the trend of Ru-25CV/oNF300 ≥ Ru-25CV/pNF > Ru-25CV/oNF500 > Ru-25CV/rNF > Ru-LPD/pNF, indicating the dependence of the oxidized nickel interlayers. By keeping the FE_{NH_3} to almost 100%, the Ru-25CV/oNF300 produces ammonia at rate of 3.6×10^{-7} mol s^{-1} cm^{-2} at −0.1 V. These results further demonstrate the importance of the oxidized nickel interlayer for achieving high activity in the conversion if nitrate to ammonia. It should be noted that the FE_{NH_3} is almost 100% from −0.9 V to −0.1 V on the Ru-25CV/oNF300 and Ru-25CV/pNF, compared to the previously reported NITRR performance with a significant decrease at high overpotentials.[10a,14a] The ammonia yield rate reaches to as high as $1.4 \pm 0.1 \times 10^{-6}$ mol s^{-1} cm^{-2} (or 5.4 ± 0.3 mmol h^{-1} cm^{-2}) at −0.6 V for Ru-25CV/oNF300, which exceeds most of reported state-of-the-art ammonia synthesis catalysts (Fig. S10†).[13,20] The Ru-25CV/oNF300 also exhibits durable and high NITRR performance for up to 100 h with no apparent loss in the selectivity, as shown in Fig. S11.†[15] The products were also analyzed for the presence of nitrite, hydroxylamine and hydrazine, but no significant levels were found.

Zhang and Yu demonstrated that the oxygen doping in Ru can cause stress stains, generating hydrogen radicals and promote the nitrate-to-ammonia conversion.[14a] Our recent study found that the NF substrate is crucial for efficient nitrate-to-ammonia conversion in Ru catalysts.[15] In this study, we investigated the impact of the interaction between the oxidized species of NF substrate and the Ru nanoparticles. While both the electrodeposited Ru films on NF (Ru-25CV/pNF) and the Ru-LPD drop-cast on NF (Ru-LPD/pNF) had reasonable oxygen doping levels, the electrodeposited Ru films on nickel supports with displayed significantly enhanced NITRR activity. The TEM analysis revealed that the Ni/Ru hybrids on NF substrates consist of an amorphous Ru–O–Ni matrix on the nickel foam with a Ni/NiOOH interlayer (Fig. S12†), indicating that the Ni in the Ru layer likely originates from oxidized nickel species on the nickel foam. During Ru electrodeposition, a strong interaction was formed between the Ru and Ni species, In contrast, the drop-casting Ru nanoparticles had a weaker interaction with Ni surfaces (Fig. 1d), resulting in low NITRR activity.[14b,21] The difference in activity could be attributed to the strong metal/metal oxide (nanoparticle)–support interactions on the Ru–Ni hybrid electrodes.[16,22] The lack of a strong interaction is likely the primary reason for low NITRR activity in Ru-LPD/pNF and electrodeposited Ru without Ni.[15]

The formation of the Ru–O–Ni metric structure is likely due to the presence of oxidized nickel species on the NF surface. To investigate this, we synthesized Ni/Ru hybrids on NF substrates with varying degrees of oxidized surfaces. The result showed that the Ni-OH peaks in the XPS of Ni 2p were shifted higher in the Ru-25CV/pNF and Ru-25CV/oNF300 samples, compared to the lower peak shifts in the Ru-25CV/rNF and Ru-25CV/oNF500 samples, as shown in Fig. 2b and 5b–d. The XPS results shows a similar presence of Ru^0 and Ru–O bonds in the Ru-25CV/pNF and Ru-25CV/rNF (Fig. S6 and S13†), whereas the Ru-25CV/rNF has a less shift of the Ni-OH peak to lower energy by 0.06 eV (Fig. 5b) than the Ru-25CV/pNF (0.23 eV) and Ru-25CV/oNF300 (0.31 eV). These results further demonstrate the essential of the presence of nickel oxides species on formation of the Ni/Ru interfacial bonding. This trend was consistent with the efficiency of the nitrate-to-ammonia conversion on Ni/Ru hybrids (Fig. 5a). It is believed that the increased shifts were due to the synergistic effect induced by oxidized nickel species and oxidized Ru, which enhanced the NITRR activities. The weak H adsorption on the oxidized Ni inhibits the H_2 formation, but provides H for the favorable NH_3 formation on the nearby Ru site in the Ru–O–Ni matrix with strong NO_3^- adsorption, thus promoting the activated NO_3^- to NH_3 pathway.[23] Furthermore, we found that the oxidized nickel layer did not introduce any significant resistance as indicated by the impedance spectroscopy (Fig. S14†). This suggests that oxidized nickel is crucial for the production of highly active NITRR catalysts. Additionally, the oxygen doping in Ru is also essential for nitrate-to-ammonia conversion, but Ru^{4+} is likely to be reduced during NITRR, resulting in decreasing performance, as reported in the literature.[14a] However, the oxidized nickel interlayers and the strong Ru–Ni interactions can probably stabilize Ru^{4+} and produce sustainable NITRR performance.

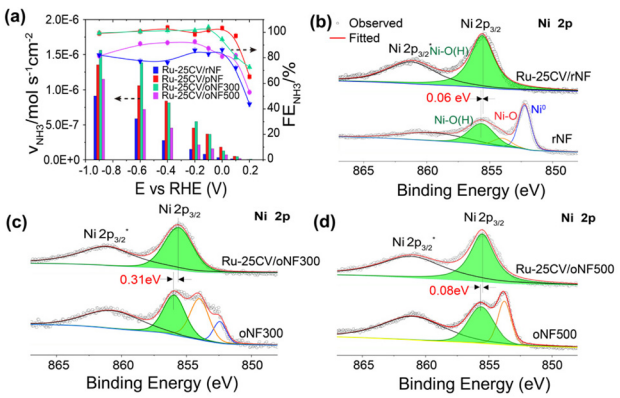

Fig. 5 (a) The ammonia yield rate (V_{NH_3}) and ammonia current faradaic efficiency (FE_{NH_3}) for Ru-25CV on different NF, measured in Ar saturated-1.0 M KOH with 1.0 M $NaNO_3$ at the scan rate of 10 mV s^{-1}. The XPS Ni 2s spectra of (b) the Ru-25CV/rNF and rNF, (c) the Ru-25CV/oNF300 and oNF300, and (d) the Ru-25CV/rNF and rNF.

Published on 19 april 2023. Downloaded on 10/11/2024 21:07:09.

Conclusions

This study found that the electrodeposition process produced a more active Ni/Ru hybrid catalyst for electrocatalytic nitrate-to-ammonia conversion than the drop-cast Ru nanoparticles on NF. This was attributed to the interaction between Ru and nickel substrate formed during electrodeposition. In addition, a series of electrodeposited Ni/Ru hybrids with different Ru loading from 0.005 to 0.055 mg cm^{-2} were synthesized on NF, which has varying oxidized surfaces. The FE_{NH_3} and V_{NH_3} follow the trend of Ru-25CV/oNF300 ≥ Ru-25CV/pNF > Ru-25CV/oNF500 > Ru-25CV/rNF > Ru-LPD/pNF. The results showed that the more oxidized NF produced more active Ni/Ru hybrids for nitrate-to-ammonia conversion due to the suppressed hydrogen evolution reaction, with the NF heat treated at 300 °C producing the highest ammonia yield rate with almost 100% faradaic efficiency. This work demonstrates the potential to enhance NITRR performance by tailoring the oxidized nickel interlayer. Further research should focus on tailoring the distribution of bi- or multi-metallic atoms at the near-surface regions to further enhance the catalytic activity and stability.

Author contributions

F. Zhou and C. S proposed the research project and analysed the data. F. Zhou conducted the experiments and drafted the manuscript. All the authors reviewed and contributed to this paper.

Conflicts of interest

There are no conflicts to declare.

Acknowledgements

F. Zhou acknowledged the funding support from National Natural Science Foundation of China (21905047) and the Guangdong Provincial Key Laboratory of Distributed Energy Systems, no. 2020B1212060075.

References

1 S. L. Foster, S. I. P. Bakovic, R. D. Duda, S. Maheshwari, R. D. Milton, S. D. Minteer, M. J. Janik, J. N. Renner and L. F. Greenlee, Catalysts for nitrogen reduction to ammonia, *Nat. Catal.*, 2018, **1**, 490–500.

2 (*a*) B. H. R. Suryanto, H.-L. Du, D. Wang, J. Chen, A. N. Simonov and D. R. MacFarlane, Challenges and prospects in the catalysis of electroreduction of nitrogen to ammonia, *Nat. Catal.*, 2019, **2**, 290–296; (*b*) X. Zhu Jr., S. Mou, Q. Peng, Q. Liu, Y. Luo, G. Chen, S. Gao and X. Sun, Aqueous electrocatalytic N_2 reduction for ambient NH_3 synthesis: recent advances in catalyst development and performance improvement, *J. Mater. Chem. A*, 2020, **8**, 1545–1556.

3 (*a*) X. Cui, C. Tang and Q. Zhang, A Review of Electrocatalytic Reduction of Dinitrogen to Ammonia under Ambient Conditions, *Adv. Energy Mater.*, 2018, **8**, 1800369; (*b*) H. K. Lee, C. S. L. Koh, Y. H. Lee, C. Liu, I. Y. Phang, X. Han, C.-K. Tsung and X. Y. Ling, Favoring the unfavored: Selective electrochemical nitrogen fixation using a reticular chemistry approach, *Sci. Adv.*, 2018, **4**, eaar3208; (*c*) W. Xu, G. Fan, J. Chen, J. Li, L. Zhang, S. Zhu, X. Su, F. Cheng and J. Chen, Nanoporous Palladium Hydride for Electrocatalytic N-2 Reduction under Ambient Conditions, *Angew. Chem., Int. Ed.*, 2020, **59**, 3511–3516; (*d*) H. Y. F. Sim, J. R. T. Chen, C. S. L. Koh, H. K. Lee, X. Han, G. C. Phan-Quang, J. Y. Pang, C. L. Lay, S. Pedireddy, I. Y. Phang, E. K. L. Yeow and X. Y. Ling, ZIF-Induced d-Band Modification in a Bimetallic Nanocatalyst: Achieving Over 44% Efficiency in the Ambient Nitrogen Reduction Reaction, *Angew. Chem., Int. Ed.*, 2020, **59**, 3511–3516; (*e*) C. Liu, Q. Li, C. Wu, J. Zhang, Y. Jin, D. R. MacFarlane and C. Sun, Single-Boron Catalysts for Nitrogen Reduction Reaction, *J. Am. Chem. Soc.*, 2019, **141**, 2884–2888; (*f*) Q. Li, S. Qiu, C. Liu, M. Liu, L. He, X. Zhang and C. Sun, Computational Design of Single-Molybdenum Catalysts for the Nitrogen Reduction Reaction, *J. Phys. Chem. C*, 2019, **123**, 2347–2352.

4 (*a*) M. Wang, S. Liu, T. Qian, J. Liul, J. Zhou, H. Ji, J. Xiong, J. Zhong and C. Yan, Over 56.55% Faradaic efficiency of ambient ammonia synthesis enabled by positively shifting the reaction potential, *Nat. Commun.*, 2019, **10**, 341; (*b*) F. Zhou, L. M. Azofra, M. Ali, M. Kar, A. N. Simonov, C. McDonnell-Worth, C. Sun, X. Zhang and D. R. MacFarlane, Electro-synthesis of ammonia from nitrogen at ambient temperature and pressure in ionic liquids, *Energy Environ. Sci.*, 2017, **10**, 2516–2520; (*c*) W. Qiu, X.-Y. Xie, J. Qiu, W.-H. Fang, R. Liang, X. Ren, X. Ji, G. Cui, A. M. Asiri, G. Cui, B. Tang and X. Sun, High-performance artificial nitrogen fixation at ambient conditions using a metal-free electrocatalyst, *Nat. Commun.*, 2018, **9**, 3485; (*d*) N. Cao, Z. Chen, K. Zang, J. Xu, J. Zhong, J. Luo, X. Xu and G. Zheng, Doping strain induced bi-Ti^{3+} pairs for efficient N_2 activation and electrocatalytic fixation, *Nat. Commun.*, 2019, **10**, 2877.

5 (*a*) Y. Liu, J. Mei, C. Shen, M. Huang, M. Yang, Z. Wang, W. Sand and F. Li, Rapid and selective electrochemical transformation of ammonia to N_2 by substoichiometric TiO_2-based electrochemical system, *RSC Adv.*, 2020, **10**, 1219–1225; (*b*) J. Choi, H.-L. Du, C. K. Nguyen, B. H. R. Suryanto, A. N. Simonov and D. R. MacFarlane, Electroreduction of Nitrates, Nitrites, and Gaseous Nitrogen Oxides: A Potential Source of Ammonia in Dinitrogen Reduction Studies, *ACS Energy Lett.*, 2020, **5**, 2095–2097; (*c*) Y. Wang, Y. Yu, R. Jia, C. Zhang and B. Zhang, Electrochemical synthesis of nitric acid from air and ammonia through waste utilization, *Natl. Sci. Rev.*, 2019, **6**, 730–738.

 This journal is © the Partner Organisations 2023

Published on 19 april 2023. Downloaded on 10/11/2024 21:07:09.

6 Q. Wang, H. Huang, L. Wang and Y. Chen, Electrochemical removal of nitrate by Cu/Ti electrode coupled with copper-modified activated carbon particles at a low current density, *Environ. Sci. Pollut. Res.*, 2019, **26**, 17567–17576.

7 M. Duca and M. T. M. Koper, Powering denitrification: the perspectives of electrocatalytic nitrate reduction, *Energy Environ. Sci.*, 2012, **5**, 9726–9742.

8 (*a*) Y. Yao, S. Zhu, H. Wang, H. Li and M. Shao, A Spectroscopic Study of Electrochemical Nitrogen and Nitrate Reduction on Rhodium Surfaces, *Angew. Chem., Int. Ed*, 2020, **59**, 10479; (*b*) G.-F. Chen, Y. Yuan, H. Jiang, S.-Y. Ren, L.-X. Ding, L. Ma, T. Wu, J. Lu and H. Wang, Electrochemical reduction of nitrate to ammonia via direct eight-electron transfer using a copper-molecular solid catalyst, *Nat. Energy*, 2020, **5**, 605–613; (*c*) H. Li, C. Yan, H. Guo, K. Shin, S. M. Humphrey, C. J. Werth and G. Henkelman, Cu_xIr_{1-x} Nanoalloy Catalysts Achieve Near 100% Selectivity for Aqueous Nitrite Reduction to NH_3, *ACS Catal.*, 2020, **10**, 7915–7921; (*d*) Y. Zeng, C. Priest, G. Wang and G. Wu, Restoring the Nitrogen Cycle by Electrochemical Reduction of Nitrate: Progress and Prospects, *Small Methods*, 2020, **4**, 2000672.

9 J. M. McEnaney, S. J. Blair, A. C. Nielander, J. A. Schwalbe, D. M. Koshy, M. Cargnello and T. F. Jaramillo, Electrolyte Engineering for Efficient Electrochemical Nitrate Reduction to Ammonia on a Titanium Electrode, *ACS Sustainable Chem. Eng.*, 2020, **8**, 2672–2681.

10 (*a*) Y. Wang, A. Xu, Z. Wang, L. Huang, J. Li, F. Li, J. Wicks, M. Luo, D.-H. Nam, C.-S. Tan, Y. Ding, J. Wu, Y. Lum, D. Cao-Thang, D. Sinton, G. Zheng and E. H. Sargent, Enhanced Nitrate-to-Ammonia Activity on Copper-Nickel Alloys via Tuning of Intermediate Adsorption, *J. Am. Chem. Soc.*, 2020, **142**, 5702–5708; (*b*) Y.-J. Shih, Z.-L. Wu, C.-Y. Lin, Y.-H. Huang and C.-P. Huang, Manipulating the crystalline morphology and facet orientation of copper and copper-palladium nanocatalysts supported on stainless steel mesh with the aid of cationic surfactant to improve the electrochemical reduction of nitrate and N_2 selectivity, *Appl. Catal., B*, 2020, **273**, 119053; (*c*) Y. L. Zhao, Y. Liu, Z. J. Zhang, Z. K. Mo, C. Y. Wang and S. Y. Gao, Flower-like open-structured polycrystalline copper with synergistic multi-crystal plane for efficient electrocatalytic reduction of nitrate to ammonia, *Nano Energy*, 2022, **97**, 7.

11 J. Gao, B. Jiang, C. Ni, Y. Qi, Y. Zhang, N. Oturan and M. A. Oturan, Non-precious Co_3O_4-TiO_2/Ti cathode based electrocatalytic nitrate reduction: Preparation, performance and mechanism, *Appl. Catal., B*, 2019, **254**, 391–402.

12 Y. Wang, W. Zhou, R. Jia, Y. Yu and B. Zhang, Unveiling the Activity Origin of a Copper-based Electrocatalyst for Selective Nitrate Reduction to Ammonia, *Angew. Chem., Int. Ed.*, 2020, **59**, 5350–5354.

13 L. Z. Sun and B. Liu, Mesoporous PdN Alloy Nanocubes for Efficient Electrochemical Nitrate Reduction to Ammonia, *Adv. Mater.*, 2023, **35**, 8.

14 (*a*) J. Li, G. Zhan, J. Yang, F. Quan, C. Mao, Y. Liu, B. Wang, F. Lei, L. Li, A. W. M. Chan, L. Xu, Y. Shi, Y. Du, W. Hao, P. K. Wong, J. Wang, S.-X. Dou, L. Zhang and J. C. Yu, Efficient Ammonia Electrosynthesis from Nitrate on Strained Ruthenium Nanoclusters, *J. Am. Chem. Soc.*, 2020, **142**, 7036–7046; (*b*) K. Liu, X. Zhao, G. Ren, T. Yang, Y. Ren, A. F. Lee, Y. Su, X. Pan, J. Zhang, Z. Chen, J. Yang, X. Liu, T. Zhou, W. Xi, J. Luo, C. Zeng, H. Matsumoto, W. Liu, Q. Jiang, K. Wilson, A. Wang, B. Qiao, W. Li and T. Zhang, Strong metal-support interaction promoted scalable production of thermally stable single-atom catalysts, *Nat. Commun.*, 2020, **11**, 1263.

15 F. Zhou and C. Sun, Nitrate-to-Ammonia Conversion on Ru/Ni Hydroxide Hybrid through Zinc-Nitrate Fuel Cell, *Small*, 2022, **18**, 2200436.

16 S. Hu and W.-X. Li, Theoretical Investigation of Metal-Support Interactions on Ripening Kinetics of Supported Particles, *ChemNanoMat*, 2018, **4**, 510–517.

17 A. M. Hengne, A. K. Samal, L. R. Enakonda, M. Harb, L. E. Gevers, D. H. Anjum, M. N. Hedhili, Y. Saih, K.-W. Huang and J.-M. Basset, Ni–Sn-Supported ZrO_2 Catalysts Modified by Indium for Selective CO_2 Hydrogenation to Methanol, *ACS Omega*, 2018, **3**, 3688–3701.

18 M. Grdeń, M. Alsabet and G. Jerkiewicz, Surface Science and Electrochemical Analysis of Nickel Foams, *ACS Appl. Mater. Interfaces*, 2012, **4**, 3012–3021.

19 M. C. Biesinger, L. W. M. Lau, A. R. Gerson and R. S. C. Smart, The role of the Auger parameter in XPS studies of nickel metal, halides and oxides, *Phys. Chem. Chem. Phys.*, 2012, **14**, 2434–2442.

20 (*a*) N. Zhang, J. Shang, X. Deng, L. J. Cai, R. Long, Y. J. Xiong and Y. Chai, Governing Interlayer Strain in Bismuth Nanocrystals for Efficient Ammonia Electrosynthesis from Nitrate Reduction, *ACS Nano*, 2022, **16**, 4795–4804; (*b*) D. Chen, S. C. Zhang, D. Yin, W. P. Li, X. M. Bu, Q. Quan, Z. X. Lai, W. Wang, Y. Meng, C. T. Liu, S. Yip, F. R. Chen, C. Y. Zhi and J. C. Ho, Tailored p-Orbital Delocalization by Diatomic Pt-Ce Induced Interlayer Spacing Engineering for Highly-Efficient Ammonia Electrosynthesis, *Adv. Energy Mater.*, 2023, **13**, 11; (*c*) F. Lv, M. Z. Sun, Y. P. Hu, J. Xu, W. Huang, N. Han, B. L. Huang and Y. G. Li, Near-unity electrochemical conversion of nitrate to ammonia on crystalline nickel porphyrin-based covalent organic frameworks, *Energy Environ. Sci.*, 2023, **16**, 201–209.

21 Q. Fu, W.-X. Li, Y. Yao, H. Liu, H.-Y. Su, D. Ma, X.-K. Gu, L. Chen, Z. Wang, H. Zhang, B. Wang and X. Bao, Interface-Confined Ferrous Centers for Catalytic Oxidation, *Science*, 2010, **328**, 1141–1144.

22 (*a*) Q. Fu, F. Yang and X. Bao, Interface-Confined Oxide Nanostructures for Catalytic Oxidation Reactions, *Acc. Chem. Res.*, 2013, **46**, 1692–1701; (*b*) J. Xia, M. Volokh, G. Peng, Y. Fu, X. Wang and M. Shalom, Low-Cost Porous Ruthenium Layer Deposited on Nickel Foam as a Highly Active Universal-pH Electrocatalyst for the Hydrogen Evolution Reaction, *ChemSusChem*, 2019, **12**, 2780–2787.

23 (*a*) F.-Y. Chen, Z.-Y. Wu, S. Gupta, D. J. Rivera, S. V. Lambeets, S. Pecaut, J. Y. T. Kim, P. Zhu, Y. Z. Finfrock, D. M. Meira, G. King, G. Gao, W. Xu, D. A. Cullen, H. Zhou, Y. Han, D. E. Perea, C. L. Muhich and H. Wang, Efficient conversion of low-concentration nitrate sources into ammonia on a Ru-dispersed Cu nanowire electrocatalyst, *Nat. Nanotechnol.*, 2022, **17**, 759; (*b*) M. Gong, D.-Y. Wang, C.-C. Chen, B.-J. Hwang and H. Dai, A mini review on nickel-based electrocatalysts for alkaline hydrogen evolution reaction, *Nano Res.*, 2016, **9**, 28–46.

Published on 19 april 2023. Downloaded on 10/11/2024 21:07:09.

This journal is © the Partner Organisations 2023